ECS Transactions, 35 (4) 259-272 (2011)
10.1149/1.3572288 ©The Electrochemical Society

Negative Charge in Plasma Oxidized SiO_2 Layers

A. Boogaard, A.Y. Kovalgin and R.A.M. Wolters

MESA+ Institute for Nanotechnology, Chair of Semiconductor Components,
University of Twente, P.O. Box 217, 7500 AE Enschede, The Netherlands.
Email: a.y.kovalgin@utwente.nl

Silicon dioxide (SiO_2) gate dielectric layers (4-60 nm thick) were deposited (0.6 nm/min) on *n*-type Si by inductively-coupled plasma-enhanced chemical vapor deposition (ICPECVD) in strongly diluted silane plasmas at 150°C . In contrast to the well-accepted positive charge for thermally grown SiO_2, the net oxide charge was negative and a function of the layer thickness. Our experiments suggested that the negative charge was created due to unavoidable oxidation of the silicon surface by plasma species, and the CVD component adding a positive space charge to the deposited oxide. The net charge was negative under process conditions where plasma oxidation played a major role. Such conditions included low deposition rates and relatively thin grown layers. Additional measurements showed that the negative charge in SiO_2 also persisted on *p*-type substrates. We suggest that plasma oxidation of the silicon surface results in SiO_2 layers with a surplus of oxygen. This surplus of oxygen is able to accumulate a negative charge. This assumption is addressed in this paper by a review of earlier work on silicon oxidation, and by a first series of experiments wherein oxygen is implanted into thermal SiO_2. It is shown that the implantation can result in a negative charge to the bulk oxide layer. The effect of the negative charge on the flatband voltage can be described by the implantation profile.

Introduction

Present-day semiconductor device manufacturing involves hundreds of process steps. Many of these steps are carried out at high temperatures, between 400 and 1000 ˚C. There is however a great demand for lower temperature processing. An expanded number of electronic devices (e.g., thin film transistors (TFT), non-volatile memory cells (NVM), MEMS/MOEMS, etc.) can be realized when lower temperatures (20-400 ˚C) are applied to the manufacturing process. One of the needs is to produce gate dielectrics (e.g. silicon dioxide – SiO_2) at low substrate temperatures. The temperature reduction normally leads to deterioration of the electrical and physical characteristics of SiO_2 layers such as leakage currents, dielectric strength, fixed and mobile oxide charge, defect density at the interface with silicon, etc.

In our previous study, we deposited SiO_2 films by Ar-N_2O-SiH_4 ICPECVD at 150°C, and a total pressure of 1-6 Pa. For the best-quality films, the gas-phase contained 0.08% of SiH_4 and 18% of N_2O. The films exhibited excellent *I-V* characteristics and low

Downloaded 28 Jul 2011 to 130.89.194.102. Redistribution subject to ECS license or copyright; see http://www.ecsdl.org/terms_use.jsp

interface state densities (D_{it}) [1-2]. These oxides were applied as gate dielectrics in low-temperature TFTs and demonstrated competitive mobility values and low off-currents.

In contrast to thermally grown SiO_2, in our ICPECVD-oxide the net charge appeared to be negative and a function of layer thickness [2]. We demonstrated that two mechanisms contributed to the film growth and charge formation, namely plasma oxidation of the silicon substrate and chemical vapor deposition. We suggested that the first nm-range of oxide thickness is formed by plasma oxidation that resulted in a negatively-charged interfacial oxide layer, while the CVD component added a positive charge to the bulk oxide.

In the current work, we extended the earlier results presented in [2] with a series of new experiments to better understand the physical nature of the negative charge observed in the ICPECVD-SiO_2 films. The negative charge might be of interest because of its novelty and the possible utilization in particular applications, e.g., for the reduction of surface recombination losses in photovoltaic devices by electrostatically shielding the minority charge carriers using internal electric fields [3].

Experimental

For this study, SiO_2 films were grown by means of ICPECVD in Ar-N_2O-SiH_4 plasma at 150°C and at a total pressure of 1 Pa, as described in [2, 4]. The gas phase contained 0.08% of SiH_4 and 18% of N_2O.

The films were deposited on H-terminated Si-wafers (*n*- or *p*-type <100>) that received standard cleaning. First, fuming nitric acid (HNO_3 100%) and boiling nitric acid (NHO_3 69%) were used in order to remove organic and metallic contaminants. The cleaning process was concluded by a 1% HF dip in order to remove the native silicon oxide. The substrates were rinsed with de-ionized water after all cleaning steps. The SiO_2 deposition process was monitored *in situ* using a J.A. Woollam M2000 spectroscopic ellipsometer (SE) with near-infrared (NIR) extension, to determine evolution of the layer thickness in time.

To electrically characterize the films, metal-oxide-semiconductor (MOS) capacitors were implemented by sputtering 1−μm Al over the oxide, followed by lithography and etching processes to define 0.06, 0.1, and 0.2 mm^2 square capacitors. An Al layer was also sputtered on the backside of the Si wafer. Some wafers were subjected to post-metallization annealing (PMA) for 10 min at 400°C in humid, ambient N_2 (N_2 bubbled through de-ionized water at room temperature). Selected wafers received a post-oxidation anneal (POA) in N_2 at 900°C for 30 min prior to the Al metallization.

The charges in thin SiO_2 films were detected by measuring their capacitance-voltage (*C-V*) characteristics. The high-frequency *C-V* measurements of the MOS structures were carried out by superimposing a small ac signal (10 kHz – 1 MHz) on a ramped dc bias between the Al gate and the substrate, by using a Hewlett-Packard 4275A multi-frequency meter. The quasi-static *C-V* curves were measured with a Hewlett-Packard 4140B pA meter, by applying only a dc bias with a sweep rate of 0.1 V/s. The bias was

Downloaded 28 Jul 2011 to 130.89.194.102. Redistribution subject to ECS license or copyright; see http://www.ecsdl.org/terms_use.jsp

applied to the metal gate. The measurements started in inversion through depletion to accumulation, then back through depletion to inversion.

Results and Discussion

In Figure 1, *in situ* SE measurements (i.e., real-time observation of the SiO_2 growth) are presented from two experiments. The first experiment (open circles) represents the first few minutes of a typical deposition process in Ar-N_2O-SiH_4 plasma. Whereas the second experiment (solid triangles) is carried out without SiH_4 in the gas phase, i.e., in Ar-N_2O plasma. Clearly, the oxide growth can also be observed without SiH_4, i.e., by plasma oxidation (solid triangles). This leads to the conclusion that (at these process conditions) the formation of silicon dioxide films is due to two mechanisms: oxidation and CVD. The inset of Figure 1 shows the calculated growth rates of the oxidation- and CVD-components. One can observe a non-linear fast-initial oxide-growth regime that gradually transfers into a linear regime with a constant deposition rate of 0.6 nm/min. We conclude that initial oxide formation is due to the oxidation of Si. Plasma oxidation dominates for the first 2.5 nanometers of the oxide growth, followed by mainly CVD for the thicker layers.

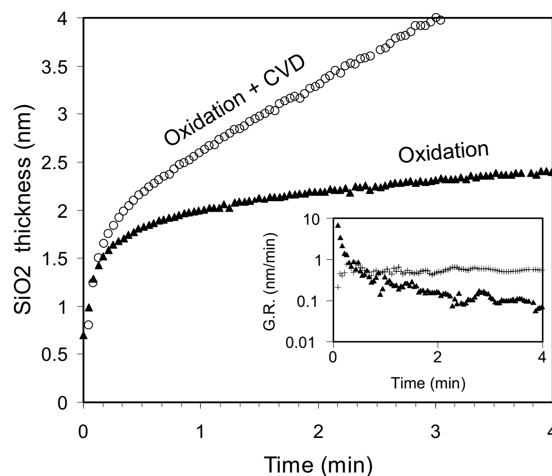

Fig. 1. *In situ* SE thickness measurements without (▲) and with (o) silane (0.08%). In the inset, the growth rates are shown for the CVD (+) and oxidation (▲) components.

One can expect the electrical properties to vary for the layers formed by the two different mechanisms. This variation can be observed particularly for very thin layers, when thicknesses of the two differently formed sub-layers are comparable. Instead of a positive charge, as normally is observed in SiO_2 films, a *negative* oxide charge of $5 \cdot 10^{11}$ cm^{-2} can be calculated from the high-frequency *C-V* curves [2].

The oxide charge is studied in more detail as a function of the layer thickness. The extracted value of the oxide charge is largely dependent on the absolute value of the metal-semiconductor workfunction difference, φ_{ms}. There is however variation in published φ_{ms} values. As an example, for Al on n-type Si with a doping level of $1.5 \cdot 10^{15}$

Downloaded 28 Jul 2011 to 130.89.194.102. Redistribution subject to ECS license or copyright; see http://www.ecsdl.org/terms_use.jsp

cm^{-3}, Sze [5] published a value of -0.2 V while Pierret [6] reported -0.3 V. To determine φ_{ms} for our system, φ_{ms} was measured on thermally grown oxide (dry oxidation at 950°C followed by 20-min POA). For thermally grown oxides, the flatband voltage can be calculated using the standard expression:

$$V_{FB} = \varphi_{ms} - \frac{Q_f T_{ox}}{K_{ox}\varepsilon_0}, \quad (1)$$

where Q_f is the fixed charge near the Si-SiO_2 interface, T_{ox} is the oxide thickness, K_{ox} is the oxide dielectric constant and ε_0 is the permittivity of vacuum.

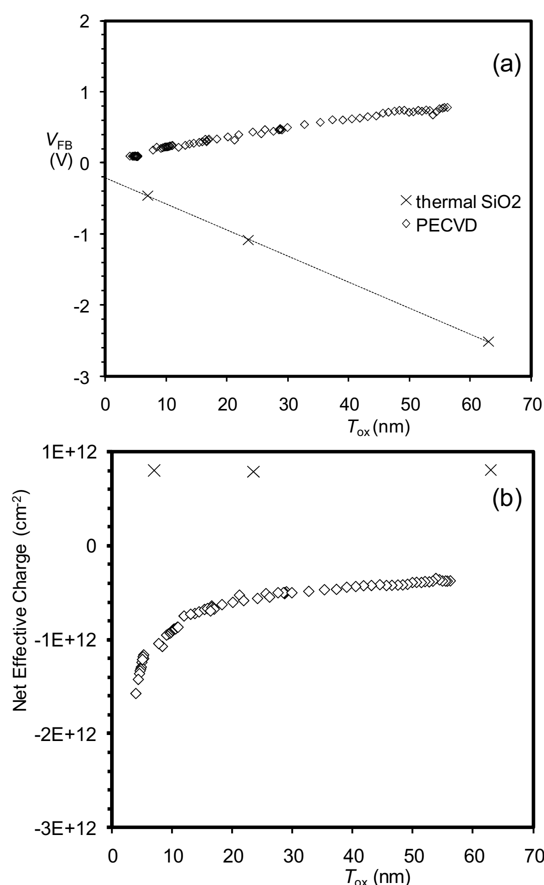

Fig. 2. Flatband voltage (a) and Net Oxide Charge (b) plotted versus oxide thickness; n-type substrates and Al-gates; after PMA. (X) Reference oxides grown by dry oxidation at 950°C followed by a POA; (◊) the ICPECVD oxides. The slope of the dotted line is proportional to the fixed charge while the intercept equals φ_{ms}.

Figure 2 shows a plot of V_{FB} versus oxide thickness for thermally grown oxides, and for our ICPECVD layers. If we compare the curves of thermal oxides and the ICPECVD oxides in Figure 2a, we observe different signs of the slopes, indicating positive and negative net-charges. The data set of thermally grown oxides has a slope of $-Q_f\, T_{ox}/K_{ox}\varepsilon_0$ and an intercept on the V_{FB} axis of $\varphi_{ms} = -0.214$ V (Q_f is assumed to be the same and near

Downloaded 28 Jul 2011 to 130.89.194.102. Redistribution subject to ECS license or copyright; see http://www.ecsdl.org/terms_use.jsp

the Si interface for all data points) [7]. The φ_{ms} thus obtained can be used to calculate Q_f. These values are shown in Figure 2b. A *positive* charge of $8{\cdot}10^{11}$ cm^{-2} was calculated for the thermally grown oxide (see crosses in Figure 2b). If Q_{ox} is calculated for the given ICPECVD oxides using the expression above, it appears that the thinner layers contain a higher amount of negative charge compared to the thicker films (see open diamonds in Figure 2b). We attribute this important and novel result to the initial plasma oxidation step, which cannot be avoided (see Fig. 1). Thus, the plasma-oxidized region near the Si-interface becomes dominant for thinner layers. This plasma oxide may therefore be responsible for the negative charge formation.

The effect of the negatively charged plasma oxide on flatband voltage can be described by general equation:

$$V_{\mathrm{FB}} = \varphi_{\mathrm{ms}} - \frac{1}{C_{\mathrm{ox}}}\int_0^{T_{\mathrm{ox}}} \frac{x}{T_{\mathrm{ox}}}\rho_{\mathrm{ox}}(x)dx, \tag{2}$$

where x is the distance from the gate, T_{ox} is the thickness of the oxide, and $\rho_{ox}(x)$ is the oxide charge density in a volume [8]. A determination of the charge distribution and its location in the oxide is needed to solve the integral. For that, we assume a homogeneous distribution of the negative charge density (ρ_{PO}) in oxide volume between the silicon interface, $x = T_{ox}$, and $x = T_{ox} - T_{PO}$, where T_{PO} is the thickness of the plasma-oxidized region (see Figure 3). Integrating reveals

$$V_{\mathrm{FB}}^{\mathrm{PO}} = \frac{\rho_{\mathrm{PO}}T_{\mathrm{PO}}(2T_{\mathrm{ox}} - T_{\mathrm{PO}})}{2C_{\mathrm{ox}}T_{\mathrm{ox}}}, \tag{3}$$

where $V_{\mathrm{FB}}^{\mathrm{PO}}$ is the flatband voltage change due to the plasma oxide. Equation (3) simplifies to Q_{PO}/C_{ox} when T_{ox} is much larger than T_{PO} ($Q_{PO} = \rho_{PO}{\cdot}T_{PO}$).

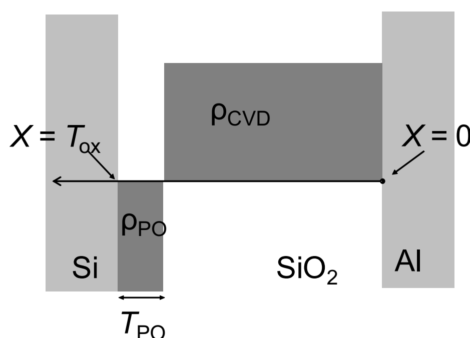

Fig. 3. Graphical representation of the suggested double-layer model. To clarify the actual (inhomogeneous) charge distribution, an additional study is required.

The pure CVD component adds the expected positive charge, thus compensating for the interface-located negative charge (the thicker the film, the more negative charge is compensated). To describe the effect of the positively charged CVD oxide on flatband voltage, we assume a homogeneous distribution of the positive charge density (ρ_{CVD}) in the volume between the gate, $x = 0$, and $x = (T_{ox} - T_{PO})$, see Figure 3.

Downloaded 28 Jul 2011 to 130.89.194.102. Redistribution subject to ECS license or copyright; see http://www.ecsdl.org/terms_use.jsp

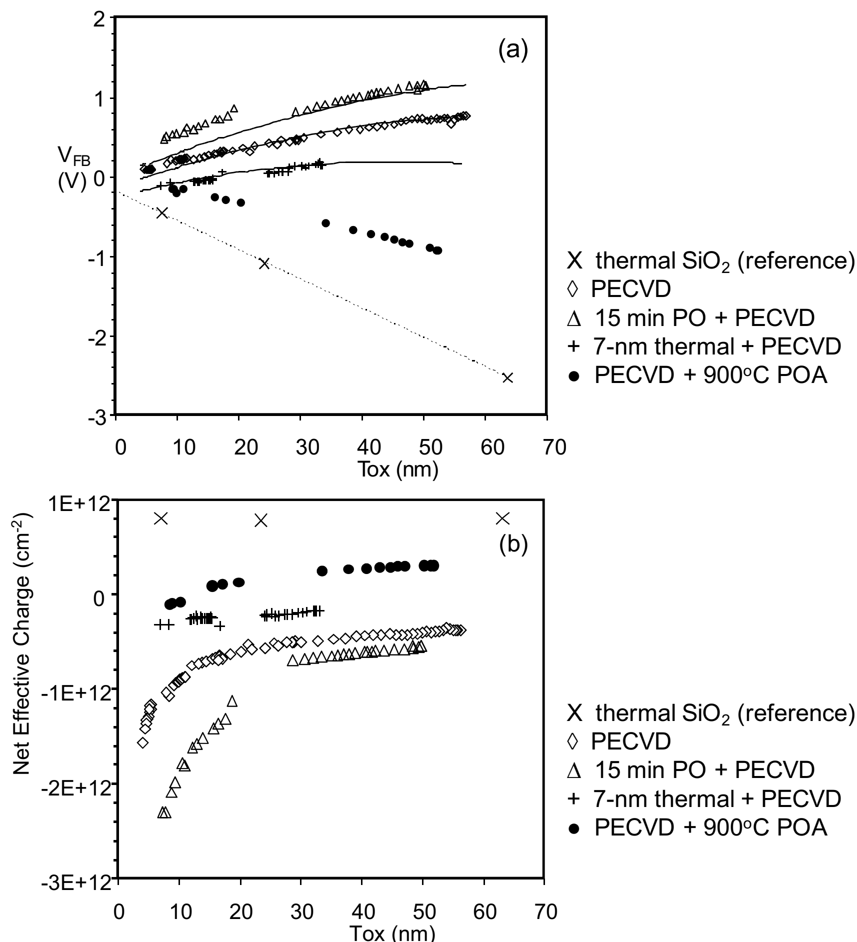

Fig. 4. Flatband voltage (a) and Net Oxide Charge (b) plotted versus oxide thickness; n-type substrates and Al-gates; after PMA. (X) Reference oxides grown by dry oxidation at 950°C followed by a POA; (◊) ICPECVD oxides; (Δ) 15-min plasma oxidation followed by ICPECVD; (+) ICPECVD oxides deposited on 7-nm thick thermal SiO_2; (●) ICPECVD oxides with POA and PMA. The slope of the dotted line is proportional to the fixed charge while the intercept equals φ_{ms}. Solid lines represent double-layer model fitting (see text).

Integrating equation (2) reveals

$$V_{\mathrm{FB}}^{\mathrm{CVD}} = \frac{\rho_{\mathrm{CVD}}(T_{\mathrm{ox}} - T_{\mathrm{PO}})^2}{2C_{\mathrm{ox}}T_{\mathrm{ox}}}, \qquad (4)$$

where $V_{\mathrm{FB}}^{\mathrm{CVD}}$ is the flatband voltage change due to the CVD oxide. Equation (4) simplifies to $Q_{\mathrm{CVD}}/2C_{\mathrm{ox}}$ for $T_{\mathrm{ox}} >> T_{\mathrm{PO}}$ ($Q_{\mathrm{CVD}} = \rho_{\mathrm{CVD}} \cdot T_{\mathrm{ox}}$). A uniform charge distribution can occur if defects, such as silicon dangling bonds or plasma damage, are continuously added to the oxide during its deposition.

The effect of the two layers on the flatband voltage can now be calculated. The double layer model fits our data (open diamonds in Figure 4a) given a *negative* oxide

Downloaded 28 Jul 2011 to 130.89.194.102. Redistribution subject to ECS license or copyright; see http://www.ecsdl.org/terms_use.jsp

charge density ρ_{PO} of $2.3\cdot10^{18}$ cm^{-3} within T_{PO}=2.5 nm, and a *positive* space charge density ρ_{CVD} of $9\cdot10^{16}$ cm^{-3}.

We further performed additional experiments to confirm the suggested double-layer model. These are presented in Figure 4. The results of thermally grown oxide and our standard ICPECVD process are included in Figure 4 for reasons of clarity. In a first experiment, initial oxide was grown by plasma oxidation only, i.e., in Ar-N_2O plasma without SiH_4. After 15 minutes of oxidation, SiH_4 was introduced into the system and the ICPECVD mode was thus activated. The prolonged plasma oxidation increased the flatband voltage (see open triangles in Figure 4a). Our model described this effect by an increase in T_{PO} from 2.5 to 2.9 nm with the same negative ρ_{PO} of $2.3\cdot10^{18}$ cm^{-3}, leaving the ρ_{CVD} unchanged (i.e. $9\cdot10^{16}$ cm^{-3}). The latter indicated that the pure CVD mode was not influenced.

In Fig. 4, one can notice a mismatch between the open triangles for T_{ox} in the range between 20 and 30 nm. This is due to the fact that two separate-in-time series of experiments were used to plot the entire curve. As the amount of negative charge is very sensitive to the initial PO step, a small deviation in the PO conditions between the series could cause the observed mismatch. Only the triangles for T_{ox} > 30 nm were used for fitting.

In a second experiment, we performed ICPECVD on a 7-nm thick thermally grown SiO_2, to minimize the influence of the initial plasma oxidation step (see plus signs in Figure 4a and Figure 4b). We obtained much less negative-charge (ρ_{PO} of $5\cdot10^{17}$ cm^{-3}) again without changing ρ_{CVD}, which reflected a similar trend of the flatband voltage in relation to oxide thickness. However, the net effective charge was still negative, indicating that plasma oxidation could not be ruled out completely.

The negative charge can be reduced during POA (see solid circles in Figure 4b), resulting in a net effective positive charge for the thicker layers (15-50 nm). However, the charge for thinner layers remains negative.

Negative effective charges were reported occasionally in PECVD silicon oxides when relatively thin layers (10-50 nm) were deposited in highly-diluted plasmas at low deposition rates [9-11]. Negative charges were also reported for silicon dioxide layers grown solely by plasma oxidation [12-13]. These publications support our conclusion on the influence of plasma oxidation on the oxide charge that always occurs parallel to deposition. With this in mind, a detailed study and model of oxidation mechanisms is needed. The majority of the PECVD oxide layers are deposited at much higher rates, and films are usually (considerably) thicker. These conditions are expected to minimize the influence of plasma oxidation, and a positive oxide charge is likely to be measured.

The electronic nature of the negative charge

Additional measurements showed the impossibility to de-trap the negative charge by applying a negative voltage to the Al gate. This indicates that charge traps, that accumulate the negative charge in our material, have energy levels in the SiO_2 band gap situated below the Fermi level of a substrate, see Figure 5. For *n*-type Si (the experiments

Downloaded 28 Jul 2011 to 130.89.194.102. Redistribution subject to ECS license or copyright; see http://www.ecsdl.org/terms_use.jsp

described above), the electron traps may lie i) within Si band gap (blue levels), or ii) below the Si valence band offset (red levels). The next step would be to narrow down this energy interval. For case i), one should observe no negative charge accumulation on *p*-type substrates. Figure 6 however indicates that the negative charge in SiO_2 persists on *p*-type substrates. Therefore, we conclude that the charge trap levels are located below the Si valence band edge (red levels).

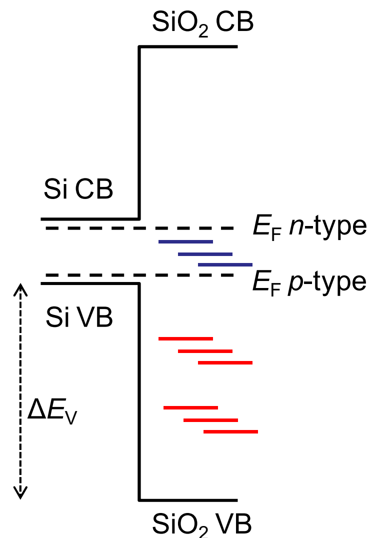

Fig. 5. Energy band diagram of the Si-SiO_2 structure under flatband conditions; $\Delta E_v = 4.4$ eV [14].

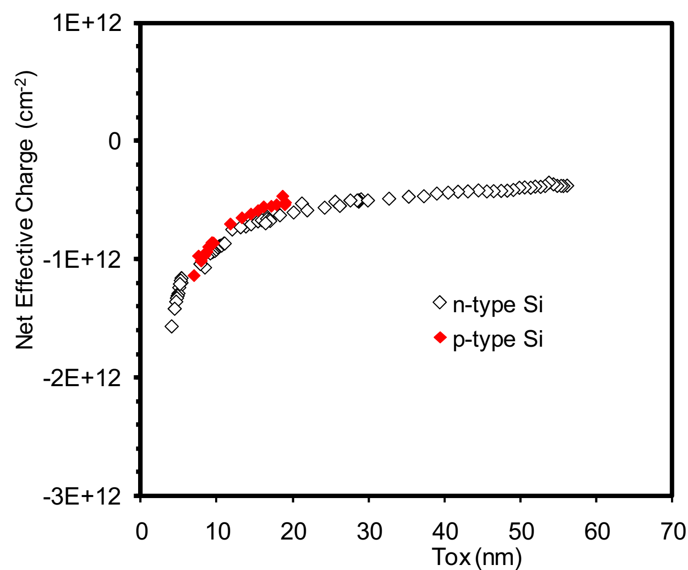

Fig. 6. Net Oxide Charge plotted versus oxide thickness; *n*-type and *p*-type substrates and Al-gates; after PMA.

Downloaded 28 Jul 2011 to 130.89.194.102. Redistribution subject to ECS license or copyright; see http://www.ecsdl.org/terms_use.jsp

The physical nature of the negative charge

During the last two decades, a number of theoretical models of silicon oxidation in the ultra-thin regime were constructed in order to surpass limitations of the commonly used Deal-Grove model. The Beck-Majkusiak model gives precise predictions even for ultrathin oxide thickness regime, for both classical oxidation in a furnace and processing in a rapid thermal oxidation (RTO) reactor, and is consistent with description of plasma oxidation processes [15]. The Beck-Majkusiak model assumes that the oxidation rate in the first phases is limited by equilibrium between the forward flux of tunneled or thermo-emitted electrons, ionizing oxygen atoms at the outer SiO_2 surface, and the return flux of the ionized species that diffuses back to Si through the already grown oxide. According to the model, the volume of SiO_2 should be full of negatively ionized oxygen atoms. If one would suddenly freeze this distribution, the total effective charge density should then be negative. This cannot be confirmed experimentally for thermal oxidation since the high temperature will also anneal and reduce the negative charge. This is also true for our ICPECVD layers, which exhibit a positive charge after POA; see solid circles in Figure 4b. For the experiments without POA, however, the temperature is much lower, which may lead to the 'freezing' effect.

Therefore, the existence of the negative charge can be related to a surplus of oxygen in the PO layer. The extra (over-stoichiometric) oxygen can be incorporated e.g. in the form of a peroxy bridge (O_3≡Si–O–O–Si≡ O_3) [16], or non-bridging O atom (i.e., formation of two O_3≡Si-O• •O-Si≡ O_3 groups with oxygen dangling bonds instead of one O_3≡Si-O-Si≡ O_3 group). It is well-known that such over-stoichiometric SiO_x does not exist in thermally-oxidized layers [16], besides some peroxy bridges in a very low concentration. Over-stoichiometric SiO_x is not stable at temperatures typical for thermal oxidation. It can possibly exist in the lower-temperature materials. This is supported by our earlier study on plasma deposition of SiO_2 films at 100°C, where we measured (by XPS) a correlation between the negative charge and the O/Si ratio slightly higher than 2 for thin films [10].This is also in agreement with the work of Afanas'ev and Stesmans, who mentioned the creation of O_3≡Si-OH centers (by irradiation with 10 eV photons) as neutral traps for electrons [17].

The extra oxygen can form negatively-charged O_2^- ions after trapping electrons. The computations of Ewig and Tellinghuizen showed that O_2^- is stable against electron auto-detachment in ionic crystals [18]. Although the ICPECVD oxide is amorphous, we speculate that the O_2^- ions can also be stable within the silica network. Salh, Von Czarnowski, and Fitting have studied over-stoichiometric SiO_x by cathode-luminescence (CL) [19-21]. For that, they implanted O^+ ions into dry-oxidized SiO_2 layers. An interesting result was the multiple regular-shaped spectra in the green-near IR (500–820 nm) region. The sub-band positions corresponded to almost equidistant energy steps of about 120 meV. Based on [18], they associated their findings to the absorption and emission spectra of O_2^- ions [20].

C-V measurements of SiO_2:O layers

The presence of O_2^- (or any other form of negative ions) is expected to induce a shift of flatband voltage as measured by *C-V* measurements. Our *C-V* measurement results on the

Downloaded 28 Jul 2011 to 130.89.194.102. Redistribution subject to ECS license or copyright; see http://www.ecsdl.org/terms_use.jsp

oxygen-implanted thermal-SiO_2 samples (kindly provided by Dr. R. Sahl of Rostock University) are presented in this section. Briefly, the SiO_2-layers prepared by dry oxidation (214-nm thick) where implanted at 45 keV with O^+ at doses of 1E+16 cm^{-2}, 5E+16 cm^{-2} and 1E+17 cm^{-2}. The samples were then annealed in N_2 at 1000°C for 30 min. Further processing at $MESA^+$ involved deposition of Al through shadow masks to define capacitors, and PMA at 400°C for 10min in humid N_2.

We will start our discussion with describing the distribution of the implanted ions. The next step will be to formulate an expression that can be used to calculate the influence of the oxide charges on the measured flatband voltage, V_{FB}. It should account for Q_f at Si-SiO_2 interface, and for Q_{bulk} according to the implantation profile. Finally, the measurement results will be presented.

According to the Lindhard, Scharff, and Schiott (LSS) model [22], the ion concentration as a function of depth, $\rho_{ion}(x)$, in amorphous materials can be described by a Gaussian curve:

$$\rho_{\text{ion}}(x) = \frac{\theta}{\sqrt{2\pi}\Delta R_{\text{p}}} e\left[-\frac{\left(x - R_{\text{p}}\right)^2}{2\Delta R_{\text{p}}^2}\right] \tag{5}$$

where θ is the implantation dose (ions/cm^2), ΔR_p is the standard deviation of the Gaussian distribution (also known as projectred straggle), and R_p is the projected range (see Figure 7). R_p and ΔR_p can be calculated from the mass of the implanted ions and the target atoms, and the mass density of the target material [22]. The results of these calculations (using Silvaco TCAD tools) are summarized in Table 1 and plotted in Figure 7. The table and figure show that the maximum of the distribution can be found at approximately half the oxide thickness. Please note that the SiO_2-Si interface, located at 0.214 µm, is not included into the simulation. Oxygen atoms will be implanted at substantial concentrations into the Si, but their exact distribution in the silicon is not relevant for the considerations we make. It is important however to be aware of the effect, because such concentrations (around $5{\cdot}10^{19}$ cm^{-3} at the SiO_2-Si interface) are likely to deteriorate the interface and quality of Si, and might thus affect the *C-V* measurements. On the other hand, the damage of Si and the interface can be restored by the following annealing step at 1000°C for 30 min [23]. Choosing a lower implantation energy (e.g., 20 keV) would also minimize the effect.

Table 1. Calculated parameters used to describe the distribution of the implanted O^+ ions (with dose θ) into amorphous SiO_2.

Implantation energy		45 keV	
θ (ions/cm^2)	1E+16	5E+16	1E+17
R_p (nm)		100	
ΔR_p (nm)		36	
$\rho_{ion}(x = R_p)$ (cm^{-3})	1.1E+21	5.6E+21	1.1E+22

Downloaded 28 Jul 2011 to 130.89.194.102. Redistribution subject to ECS license or copyright; see http://www.ecsdl.org/terms_use.jsp

The expression used to calculate the influence of the oxide charges on V_{FB} should account for ρ_f ($Q_f = \rho_f \cdot T_f$) at Si-SiO$_2$ interface, and for ρ_{bulk} ($Q_{bulk} = \rho_{bulk} \cdot T_{ox}$) according to the implantation profile. The effect of the fixed charge, ρ_f, on the flatband voltage can be calculated using equation (3). To describe the effect of the negatively charged implanted oxide, having the charge density ρ_{bulk}, on flatband voltage, we insert the simulated implantation profile (equation (5)) of the oxygen atoms (ρ_{bulk}) into equation (2) (see Figure 8). Integrating reveals

$$V_{FB}^{bulk} = -\frac{1}{2}\frac{\theta\left[-\sqrt{2}\Delta R_p e^{-\frac{R_p^2}{\Delta R_p^2}} - \sqrt{\pi}R_p erf\left(\frac{\sqrt{2}R_p}{2\Delta R_p}\right) + \sqrt{2}\Delta R_p e^{-\frac{(R_p - T_{ox})^2}{\Delta R_p^2}} + \sqrt{\pi}R_p erf\left(\frac{\sqrt{2}(R_p - T_{ox})}{2\Delta R_p}\right)\right]}{\sqrt{\pi}C_{ox}T_{ox}}, \quad (6)$$

However, it is assumed that only a fraction, $f(\theta)$, of the implanted ions is electrically active as O_2^-. So, a small change in the expression is necessary: θ is to be replaced by $f(\theta) \times \theta$.

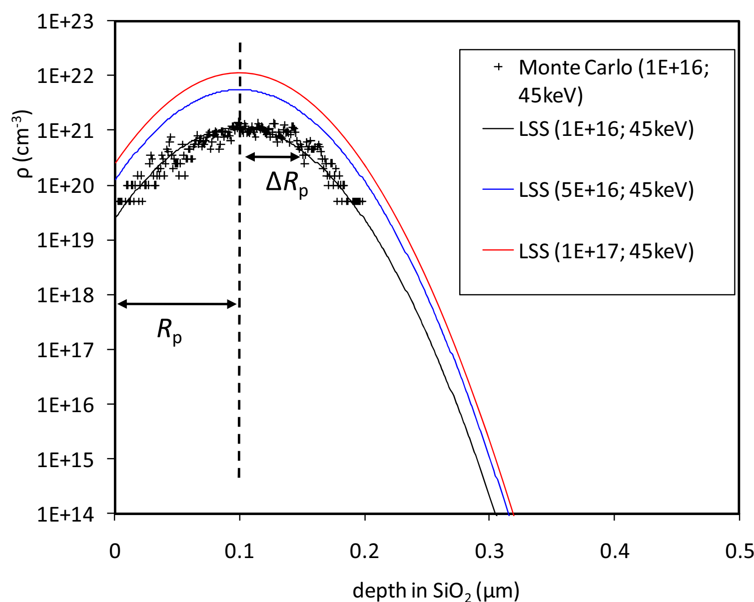

Fig. 7. The implantation profiles of O^+ implanted into amorphous SiO$_2$. The profiles are shown for both the LSS model and Monte Carlo simulations.

The measured *C-V* curves are shown in Figure 9. The figure reveals that V_{FB} of the SiO$_2$:O films is more negative than φ_{ms}. (The V_{FB} of the reference SiO$_2$ thermally grown on n-type Si and without implantation of oxygen was measured to be -0.214 V, see text under Fig. 2.) On one hand, the O^+-implanted films clearly have an increased positive effective charge (cf. equation (3) and Figure 9) compared to the reference SiO$_2$. This could be due to the mentioned deterioration of the interface after implantation. On the other hand, V_{FB} clearly shifts towards φ_{ms} for the higher implantation doses. This means that the effective positive charge is reduced when the implantation dose is increased. To explain this observation, one should bear in mind that thermal oxidation is known to create a positive charge (Q_f) near the Si-SiO$_2$ interface. This Q_f is partly compensated by

Downloaded 28 Jul 2011 to 130.89.194.102. Redistribution subject to ECS license or copyright; see http://www.ecsdl.org/terms_use.jsp

a negative charge of the over-stoichiometric oxygen ions additionally implanted into the bulk oxide. A higher implantation dose will thus reduce the effective positive charge to lower values.

The effect of the implantations on the flatband voltage can also be calculated by combining equations (3) and (6). The results are shown in Table 2. Our model can describe the measured flatband voltages by a constant Q_f of $3.2 \cdot 10^{+11}$ cm^{-2} for all the samples. This indicates that annealing can equally restored the Si-SiO_2 interface for all the films. The Q_f is partly compensated by the negatively charged oxygen atoms.

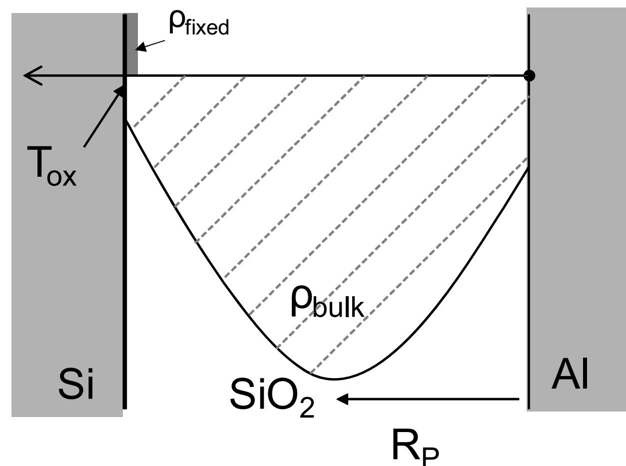

Fig. 8. Graphical representation of the charge distribution in the Si_2O:O (i.e., O^+-implanted) layer.

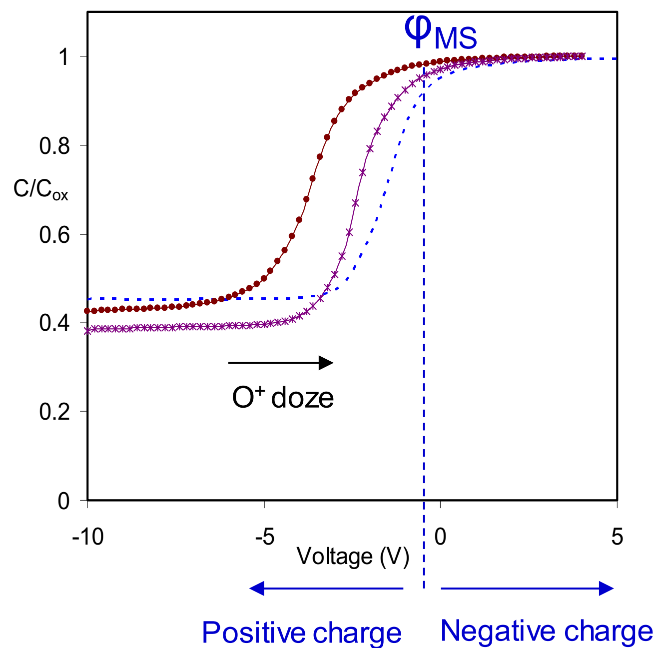

Fig. 9. Measured *C-V* curves of the SiO_2:O layers. The O^+ implantation dose (see Tables 1 and 2 for details) increases from left to right.

Downloaded 28 Jul 2011 to 130.89.194.102. Redistribution subject to ECS license or copyright; see http://www.ecsdl.org/terms_use.jsp

According to our model, only a small fraction (about $5\cdot10^{-6}$) of the implanted ions is electrically activated in the form of negatively charged ions. The negative-charge distribution can easily be found from Figure 7 by multiplying $½\cdot\rho_{bulk}$ by the activation fraction from Table 2 (½ is added because 2 implanted oxygen atoms are needed to form one O_2^-). The highest concentration (according to our model) of O_2^- is $2\cdot10^{+16}$ cm^{-3} (located at R_p and for $\theta = 1\cdot10^{+17}$ $ions/cm^2$). This is just below the maximum solubility of O_2 in SiO_2, which is $5\cdot10^{+16}$ cm^{-3} [24], and is therefore a physically feasible and relevant number.

Table 2. Calculated (based on the *C-V* data of Fig. 9) V_{FB} and Q_f as a function of the oxygen implantation dose into amorphous SiO_2.

θ (ions/cm^2)	1E+16	5E+16	1E+17
measured V_{FB} (V)	-3.09	-1.93	-0.94
modelled V_{FB} (V)	-3.08	-1.92	-0.93
$f(\theta)$ (-)	6.3E-06	5.3E-06	4.4E-6
Q_f (cm^{-2})		3.2E+11	

Conclusions

The net charge of the studied ICPECVD-SiO_2 films was found to be negative, and was a function of the film thickness. This was explained by the plasma oxidation of silicon, which added a negative charge ($2.3\cdot10^{18}$ cm^{-3}) to the interfacial oxide layer (2.5-nm thick), while the CVD-component added a nearly homogeneous distribution of a positive charge ($9\cdot10^{16}$ cm^{-3}) to the bulk oxide. The charge traps of the negatively-charged PO layer are located below the Si valence band edge.

The thermally-grown O^+-implanted SiO_2 films clarified the physical nature of the negative charge. Although the net-oxide charge was positive, it was a function of the implantation dose. Our model assumed a positive fixed charge at the interface ($3.2\cdot10^{+11}$ cm^{-2}) and a negative charge, distributed similarly to the implantation profile. We therefore attributed the negative charge to a surplus of oxygen. This over-stoichiometric oxygen was possibly able to accumulate a negative charge.

Acknowledgements

The authors are very grateful to Dr. R. Salh of Rostock University for providing the thermally-grown O^+-implanted SiO_2 samples.

References

1. I. Brunets, J. Holleman, A. Y. Kovalgin, A. Boogaard and J. Schmitz, *IEEE Transactions on Electron Devices*, **56**, 1637 (2009).

Downloaded 28 Jul 2011 to 130.89.194.102. Redistribution subject to ECS license or copyright; see http://www.ecsdl.org/terms_use.jsp

2. A. Boogaard, A. Y. Kovalgin and R. A. M. Wolters, *Microelectronic Engineering*, **86**, 1707 (2009).
3. B. Hoex, J. J. H. Gielis, M. C. M. v. d. Sanden and W. M. M. Kessels, *Journal of Applied Physics*, **104**, 113703 (2008).
4. A. Boogaard, A. Y. Kovalgin, I. Brunets, A. A. I. Aarnink, J. Holleman, R. A. M. Wolters and J. Schmitz, *Surface and Coatings Technology*, **201**, 8976 (2007).
5. S. M. Sze and K. K. Ng, in *Physiscs of Semiconductor Devices*, third edition ed., p. 197, Wiley-Interscience, New York (2007).
6. R. F. Pierret, in *Semiconductor Device Fundamentals*, p. 649, Addison Wesley Longman, Amsterdam (1996).
7. A. S. Grove, in *Physics and technology of semiconductor devices*, p. 345, John Wiley and Sons, Inc., New York (1967).
8. D. K. Schroder, in *Semiconductor material and device characterization*, 3rd ed., p. 321, John Wiley and Sons, Inc., Hoboken (2006).
9. S. S. Iyer, P. M. Solomon, V. P. Kesan, A. A. Bright, J. L. Freeouf, T. N. Nguyen and A. C. Warren, *Electron Device Letters, IEEE*, **12**, 246 (1991).
10. A. Y. Kovalgin, G. Isai, J. Holleman and J. Schmitz, *Journal of The Electrochemical Society*, **155**, G21 (2008).
11. M. J. Hernandez, J. Garrido, J. Martinez and J. Piqueras, *Semiconductor Science and Technology*, **11**, 422 (1996).
12. T. Yasuda, Y. Ma, S. Habermehl and G. Lucovsky, *Applied Physics Letters*, **60**, 434 (1992).
13. M. Tabakomori and H. Ikoma, *Japanese Journal of Applied Physics Part 1-Regular Papers Short Notes & Review Papers*, **36**, 5409 (1997).
14. J. Robertson, *Journal of Non-Crystalline Solids*, **303**, 94 (2002).
15. R. B. Beck, *Materials Science in Semiconductor Processing*, **6**, 49 (2003).
16. C. R. Helm and B. E. Deal, *The Physics and Chemistry of SiO_2 and the Si–SiO_2 Interface*, Plenum, New York (1993).
17. V. V. Afanas'ev and A. Stesmans, *Applied Physics Letters*, **71**, 3844 (1997).
18. C. S. Ewig and J. Tellinghuisen, *The Journal of Chemical Physics*, **95**, 1097 (1991).
19. H. J. Fitting, T. Barfels, A. N. Trukhin, B. Schmidt, A. Gulans and A. von Czarnowski, *Journal of Non-Crystalline Solids*, **303**, 218 (2002).
20. H. J. Fitting, R. Salh, T. Barfels and B. Schmidt, *physica status solidi (a)*, **202**, R142 (2005).
21. R. Salh, A. von Czarnowski and H. J. Fitting, *Journal of Non-Crystalline Solids*, **353**, 546 (2007).
22. J. Lindhard and M. Scharff, *Physical Review*, **124**, 128 (1961).
23. S. Wolf and R. N. Tauber, in *Silicon processing for the VLSI Era. Vol. 1. Process technology*, 1st ed., p. 198, Lattice Press, Sunset Beach (1986).
24. N. Mott, *Proceedings of the Royal Society of London. Series A, Mathematical and Physical Sciences*, **376**, 207 (1981).

Downloaded 28 Jul 2011 to 130.89.194.102. Redistribution subject to ECS license or copyright; see http://www.ecsdl.org/terms_use.jsp